
01 Jan 2023

Prediction Of Single Proppant Terminal Settling Velocity In High Viscosity Friction Reducers By Using Artificial Neural Networks And XGBoost

Xiaojing Ge

Rong Lu


Ghith Biheri

Abdulmohsin Imqam

Missouri University of Science and Technology, ahikx7@mst.edu

et. al. For a complete list of authors, see https://scholarsmine.mst.edu/geosci_geo_peteng_facwork/2178

Follow this and additional works at: https://scholarsmine.mst.edu/geosci_geo_peteng_facwork

 Part of the [Biochemical and Biomolecular Engineering Commons](#), [Geological Engineering Commons](#), and the [Petroleum Engineering Commons](#)

Recommended Citation

X. Ge et al., "Prediction Of Single Proppant Terminal Settling Velocity In High Viscosity Friction Reducers By Using Artificial Neural Networks And XGBoost," *SPE Western Regional Meeting Proceedings*, Society of Petroleum Engineers, Jan 2023.

The definitive version is available at <https://doi.org/10.2118/212964-MS>

This Article - Conference proceedings is brought to you for free and open access by Scholars' Mine. It has been accepted for inclusion in Geosciences and Geological and Petroleum Engineering Faculty Research & Creative Works by an authorized administrator of Scholars' Mine. This work is protected by U. S. Copyright Law. Unauthorized use including reproduction for redistribution requires the permission of the copyright holder. For more information, please contact scholarsmine@mst.edu.



Society of Petroleum Engineers

SPE-212964-MS

Prediction of Single Proppant Terminal Settling Velocity in High Viscosity Friction Reducers by Using Artificial Neural Networks and XGBoost

Xiaojing Ge, Missouri University of Science and Technology; Rong Lu, bp; Ghith Biheri, Abdulmohsin Imqam, and Baojun Bai, Missouri University of Science and Technology

Copyright 2023, Society of Petroleum Engineers DOI [10.2118/212964-MS](https://doi.org/10.2118/212964-MS)

This paper was prepared for presentation at the SPE Western Regional Meeting held in Anchorage, Alaska, USA, 22 - 25 May 2023.

This paper was selected for presentation by an SPE program committee following review of information contained in an abstract submitted by the author(s). Contents of the paper have not been reviewed by the Society of Petroleum Engineers and are subject to correction by the author(s). The material does not necessarily reflect any position of the Society of Petroleum Engineers, its officers, or members. Electronic reproduction, distribution, or storage of any part of this paper without the written consent of the Society of Petroleum Engineers is prohibited. Permission to reproduce in print is restricted to an abstract of not more than 300 words; illustrations may not be copied. The abstract must contain conspicuous acknowledgment of SPE copyright.

Abstract

High viscosity friction reducers (HVFRs) have been recently gaining more attention and increasing in use, not only as friction-reducing agents but also as proppant carriers. The settling velocity of the proppant is one of the key outputs to describe their proppant transport capability. However, it is influenced by many factors such as fluid properties, proppant properties, and fracture properties. Many empirical/physics-based models and correlations to predict particle settling velocity have been developed. However, they are usually based on certain assumptions and have applicable limits. In contrast, machine learning models can be considered as a black box. The objective of this study is to use machine learning models to find the relationship between the multiple factors mentioned above and particle settling velocity in order to correctly predict it. Two of the most popular and powerful machine learning algorithms, Artificial neural networks (ANN) and XGBoost, were comparatively investigated with standard data processing and training procedures. Mean Absolute Errors (MAEs) for ANNs and XGBoost were 0.010379 and 0.004253 respectively. The XGBoost learning algorithm had overall better prediction performance than the ANN model in terms of the data sets used for this study and had the potential to properly handle missing values by itself.

Introduction

Understanding proppant transport behaviors in fractures plays a significant role in hydraulic fracturing design. Proppant settling velocity is a key parameter to evaluate proppant transport performance, which is affected by three main factors including fluid properties, proppant properties, and fracture properties. For fluid properties, they may include density, viscosity, and elasticity. For proppant properties, they may include density, size, non-uniformity, surface wettability, and concentration. For fracture properties, they may include fracture width, smoothness, and complexity. From the practical viewpoint of field applications, the settling velocity of proppant is usually controlled by monitoring fluid properties and proppant properties (McCabe et al. 2004; Arnipally and Kuru 2018; Biheri and Imqam 2021a, 2021b; Ge and Imqam 2022; Yao et al. 2022).

Empirical correlations are commonly used to predict the particle-settling velocity in complex fluids. The correlation was first developed to determine particle settling velocity in a creeping flow of a Newtonian

fluid by Stokes (1851). However, most industrial applications required the use of non-Newtonian fluids. Therefore, a lot of models were developed for purely viscous non-Newtonian shear-thinning fluids to predict particle settling velocity without considering the fluid elasticity effect. According to Acharya (1988), the settling velocity of a single particle in unconfined inelastic fluids can be described the following Equations:

For $Re_{INEL} < 2$:

$$V_{INEL} = \left[\frac{(\rho_p - \rho_f)gd_p^{n+1}}{18KF(n)} \right]^{\frac{1}{n}} \quad (1)$$

$F(n)$ is the drag correction factor given by:

$$F(n) = 3^{\frac{(3n-3)}{2}} \left[\frac{33n^5 - 63n^4 - 11n^3 + 97n^2 + 16n}{4n^2(n+1)(n+2)(2n+1)} \right] \quad (2)$$

For $2 < Re_{INEL} < 500$:

$$V_{INEL} = \left\{ \frac{3\rho_f}{4(\rho_p - \rho_f)gd_p} \left[\frac{24F(n)}{4Re_{INEL}} + \frac{f_2(n)}{Re_{INEL}^{f_3(n)}} \right] \right\}^{-1/2} \quad (3)$$

$$f_2(n) = 10.5n - 3.5 \quad (4)$$

$$f_3(n) = 0.32n - 0.13 \quad (5)$$

$$Re_{INEL} = \frac{\rho_f V_{INEL}^{2-nd_p^n}}{K} \quad (6)$$

To further consider the fluid-elasticity effect, the correlation between settling velocity in elastic fluids and inelastic fluids was introduced by Malhotra and Sharma (2011) as Equations below:

$$\frac{V_{EL}}{V_{INEL}} = \frac{1 + We_{INEL}^{4.5} n^{-1.16}}{1 + We_{INEL}^5 Re_{INEL}^{0.12}} \quad (7)$$

$$We_{INEL} = \frac{2TV_{INEL}}{d_p} \quad (8)$$

$$Re_{INEL} = \frac{\rho_f V_{INEL}^{2-nd_p^n}}{K} \quad (9)$$

However, the correlation above was only applicable in the following range of variables:

$$0.39 \leq n \leq 1.0, 0 \leq We_{INEL} \leq 22, 612 \times 10^{-6} \leq Re_{INEL} \leq 6.63$$

Besides elasticity effect, the correlation for fracture wall retardation effect was also introduced by Malhotra and Sharma (2011) as the following Equations:

$$\frac{V_{ELConfined}}{V_{EL}} = (1-r)^p \quad (10)$$

$$p = 0.44We_{EL}^{-0.19} \quad (11)$$

$$We_{EL} = \frac{2TV_{EL}}{d_p} \quad (12)$$

The correlation was only valid in the following range of variables:

$$0 \leq r \leq 1, 0.39 \leq n \leq 1.0, 0.25 \leq We_{EL} \leq 9.7$$

As shown above, the empirical/physics-based models for predicting settling velocity are usually based on certain assumptions and have applicable limits. In contrast, machine learning models usually lack the fundamental physics behind the phenomenon and can be considered as a black box (Lu 2020; Abdullah et

al. 2023). In this study, we explored using machine learning as an alternative to these models to predict single proppant settling velocity in HVFRs. Two of the most popular and powerful learning algorithms, ANN and XGBoosting, were comparatively investigated.

Approach and Model Development

Dataset Collection and Quality Control

In this work, single particle settling velocity data were collected from both literature and experimental works conducted by our research group (Kelessidis 2003; Kelessidis and Mpandelis 2004; Malhotra 2010; Arnipally and Kuru 2018; Biheri and Imqam 2022; Ge and Imqam 2022). To ensure the quality of the data, we mined them from their original literature instead of the papers they were cited. It was highly recommended to do so because the original data might not be like they were cited as.

For HVFRs, they usually exhibit shear-thinning behaviors with high viscosity and elasticity under DI water conditions. However, they become more Newtonian-like with low viscosity and negligible elasticity under high-TDS and high-temperature conditions (Ge and Imqam 2022; Ge et al. 2022). Therefore, the data contain particle settling in Newtonian, non-Newtonian, elastic, and inelastic four different fluids. To predict single particle settling velocity in HVFRs, 7 input features were selected based on physics-based models and empirical correlations mentioned in the introduction section, which included flow consistency index (K), flow behavior index (n), particle diameter (d_p), density of the particle (ρ_p), density of the fluid (ρ_f), relaxation time of the fluid (T), and width of the fracture (W). K and n were used to describe fluid behavior and viscosity. The reason for not using apparent viscosity (μ) directly was that it was changing with the shear rate. T was used to describe the fluid elastic property. W was used to count the wall retardation effect. All these inputs were independent of each other based on their physical meanings, which prevented multicollinearity problems even though complex learning algorithms, such as ANN and XGBoost, could easily handle this. Redundant features were also prevented from feature selection, which could decrease the learning efficiency and cause over-fitting problems (Yu and Liu 2004). For example, the Reynolds number (Re) was not selected as an input feature because it was dependent on other features as shown in Equations (6) and (9). Totally 184 data sets were used for this study, which were shown in Table A-1 in Appendix A.

Data Preprocessing

Before constructing machine learning models to predict particle settling velocity, the original data sets were preprocessed. Firstly, missing values should be checked and properly handled. The original data sets contained certain missing values. For example, some literature did not mention fluid density and relaxation time. Since the data sets were small, these missing values were manually imputed based on the information provided within literature. However, if the data set is large, statistical measures such as mean, median, or mode can be used for imputation or interpolation can be applied. In general, it is important to choose the best imputation method based on the specific requirements of the machine learning task. Besides, some learning algorithms like XGBoost can automatically handle missing values by themselves. The training results for data with and without missing values by using XGBoost were comparatively investigated in this study. Table A-1 in Appendix A was actually the modified data sets with missing values manually imputed by the best approximation based on the information provided within literature.

Secondly, the distribution of the data sets for both input and output features was visualized as shown in Figs. 1 and 2. By looking at Fig. 1, data sparsity occurred for some features due to small data sets. By looking at Fig. 2, there were two significant outliers observed. Therefore, the data whose measured values were greater than 0.4 were regarded as outliers and removed.

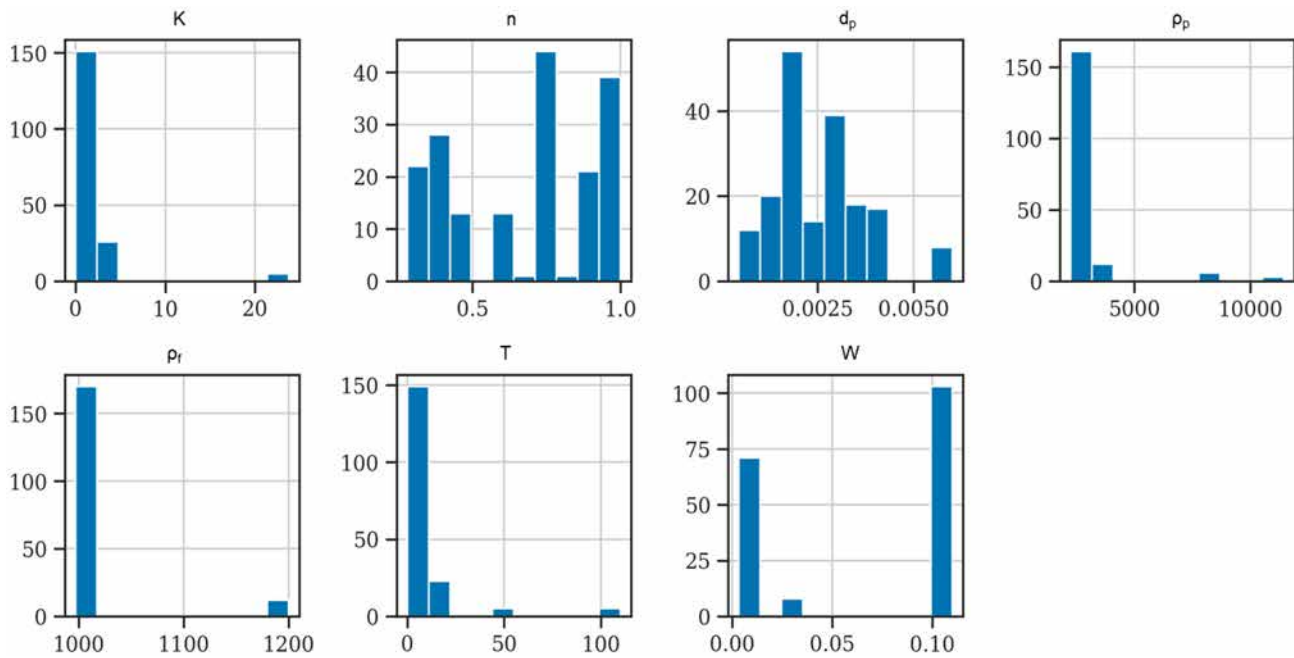


Figure 1—The frequency distribution of the input features.

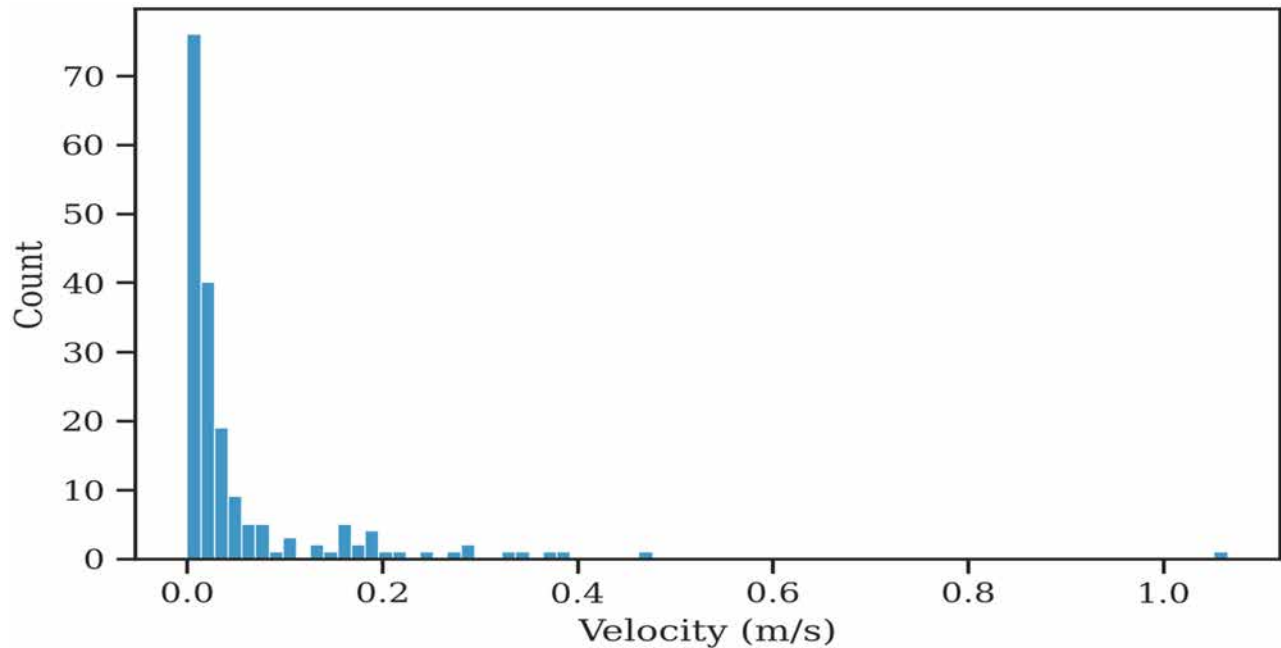


Figure 2—The frequency distribution of the output feature.

Thirdly, The Spearman correlation coefficient heat map for input and output features was shown in Fig. 3 to identify any collinearity problem. As mentioned above, it might be harmful to simple learning models, while complex learning algorithms like ANN and XGBoost can easily handle this. The relaxation time (T) showed a large negative Spearman correlation coefficient (-0.67) to flow behavior index (n). However, they are independent of each other by their physical meanings. It might be the result of small data sets.

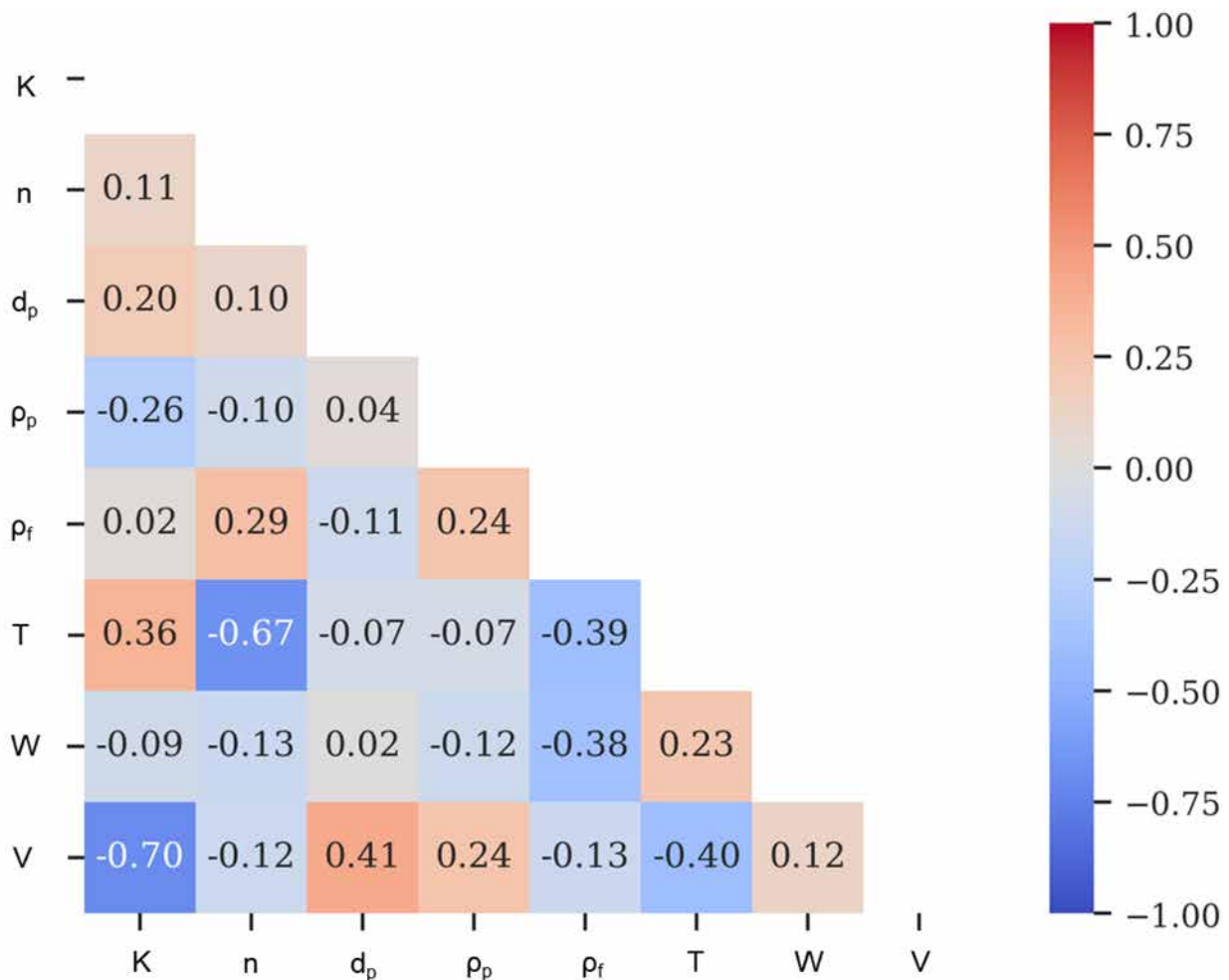


Figure 3—The Spearman correlation coefficient heat map for input and output features.

Fourthly, the data sets were divided into two parts, training data and test data, and training data accounted for 80% of the total data.

Finally, data normalization was implemented to each input feature to scale them to have comparable ranges of values to each other, which reduced the influence of the scale of different features and eliminated the bias towards features with large magnitude values.

Training Methods and Model Optimization

Two of the most popular and powerful learning algorithms, ANN and XGBoost, were comparatively investigated in this study.

ANN is a machine learning technique that is primarily inspired by the structure and function of biological neurons. It is particularly well-suited for addressing complex, nonlinear problems with multiple parameters (Zhu et al. 2021). For this study, the number of hidden layers was set to one. During the training process, parameters, including the number of neurons in the hidden layer, number of epochs, batch size, activation function, optimizer, learning rate, and momentum, were tuned and determined by the grid search technique to obtain the best model performance.

XGBoost is another powerful machine learning algorithm by implementing gradient boosting, which can make predictions by using boosting of the ensemble of weak prediction models, typically decision trees, to form a stronger and more accurate model (Rao et al. 2019). Compared to the ANN model, XGBoost works well on tabular data but is not recommended for unstructured data like images, audio, and text. The parameters tuned for XGBoost by using grid search techniques included the number of decision trees, the

depth of decision trees, learning rate, row subsampling, column subsampling by trees, column subsampling by levels, and column subsampling by nodes.

3- and 5-fold cross-validations were implemented to the ANN and XGBoost models respectively. Mean Absolute Error (MAE) was used to evaluate the performance of both models.

Results and Discussion

In general, selecting a machine learning model is a balancing act between model variance and bias. Simple models usually have a higher bias and lower variance, whereas more complex models have a lower bias and higher variance (Abdullah et al. 2023). Therefore, different models from the simplest ones like linear regression to more complex ones like XGBoost and RF were sequentially tested by using default parameters to observe the baseline performance. 10-fold cross-validation was implemented for each model and MAE results were presented in Fig. 4. As it showed, XGBoost (XGB) had the best initial performance with the lowest MAE. Then, parameters for XGBoost were further tuned with the grid search technique to obtain optimized performance.

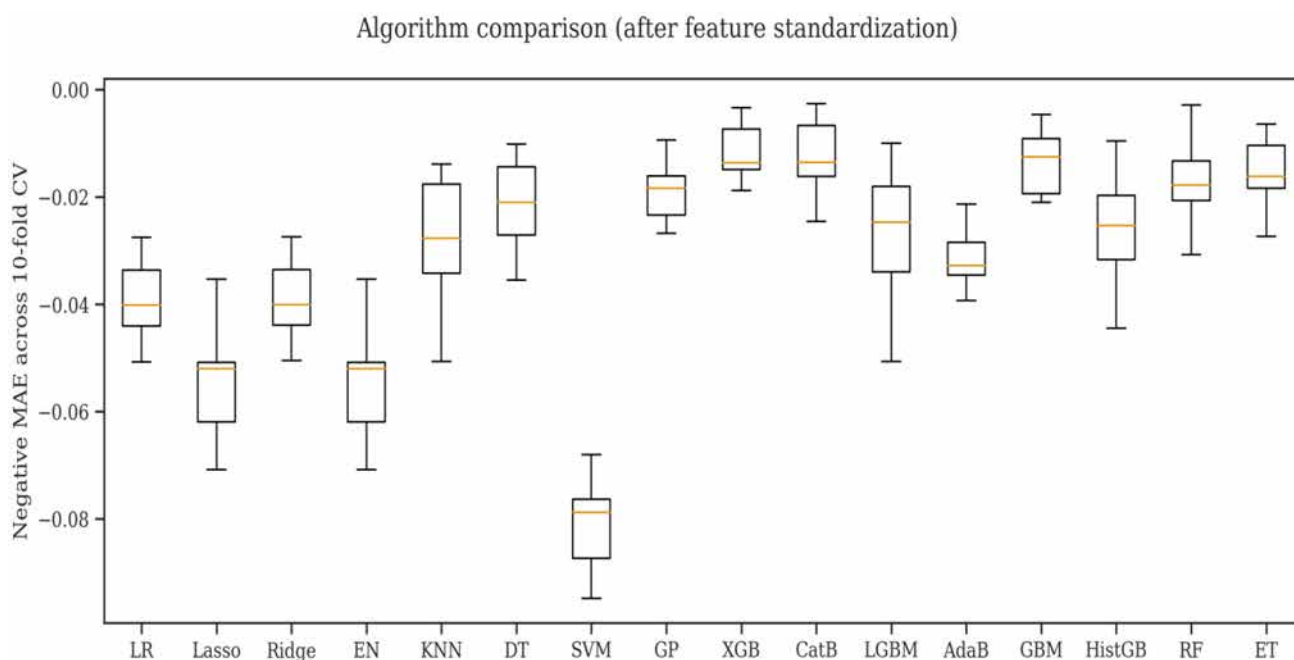
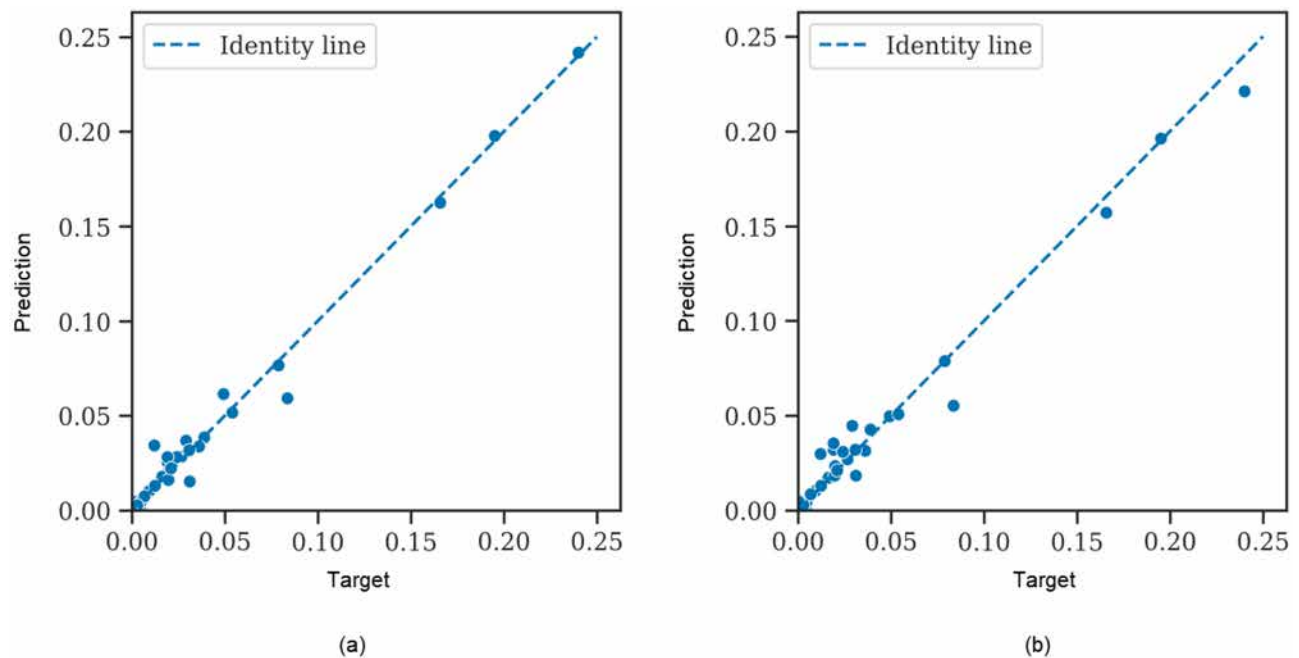


Figure 4—The Baseline performance evaluation for varies machine learning models.

Table 1 showed the parameters of the XGBoost model determined after using the grid search technique. With these determined parameters, the trained model was fit into the test datasets to reveal the predictions vs. target values as shown in Fig. 5 (a). Most of the points were closely aligned with the identity line and the MAE was 0.004253, which indicated this model performed well on predicting single proppant settling velocity. The model trained with data having missing values also fit into the test datasets as shown in Fig. 5 (b). This model also performed well on predicting settling velocity with a MAE of 0.005034, which was close to the model trained with manually imputed data. XGBoost had the potential to properly handle missing values by itself.

Table 1—Grid search ranges and results for XGBoost model parameters.

Parameter	Grid Search Ranges	Grid Search Result
Number of decision trees	100, 200, 300, 400, 500, 600, 700, 800, 900, 950, 1000	1000
Depth of decision trees	2, 3, 4, 5, 6	3
Learning rate	0.0001, 0.001, 0.01, 0.1, 0.2, 0.3	0.1
Row subsampling	0.1, 0.2, 0.3, 0.4, 0.5, 0.6, 0.7, 0.8, 0.9, 1.0	0.7
Column subsampling by trees	0.1, 0.2, 0.3, 0.4, 0.5, 0.6, 0.7, 0.8, 0.9, 1.0	1
Column subsampling by levels	0.1, 0.2, 0.3, 0.4, 0.5, 0.6, 0.7, 0.8, 0.9, 1.0	0.8
Column subsampling by nodes	0.1, 0.2, 0.3, 0.4, 0.5, 0.6, 0.7, 0.8, 0.9, 1.0	0.4

**Figure 5—Plots of predictions vs. target values with (a) manually imputed data and (b) missing-value data by using the XGBoost model.**

Similarly, Table 2 showed the parameters of the ANN model determined after using the grid search technique. With these determined parameters, the trained model was fit into the test datasets to reveal the predictions vs. target values as shown in Fig. 6. When target values were small (i.e., less than 0.05), residuals were relatively small and most of the points were closely aligned with the identity line. However, when target values were large (i.e., greater than 0.05), residuals became relatively large, and points were far away from the identity line. The main reason for this was that the outputs of datasets were right skewed as shown in Fig. 2. The model could not fully reveal the pattern for large-output datasets. The MAE for the ANN model was 0.010379, which was higher than the MAE of XGBoost. Therefore, XGBoost had better performance than ANN with one hidden layer in terms of selected datasets in this study.

Table 2—Grid search ranges and results for ANN model parameters.

Parameter	Grid Search Ranges	Grid Search Result
Number of neurons	7, 8, 12, 13, 14	7
Number of epochs	range (start = 100, stop = 1100, step = 100)	600
Batch size	2, 4, 8	2
Activation function	'sigmoid', 'relu', 'tanh'	'relu'
Optimizer	'SGD', 'RMSprop', 'Adam', 'Adamax', 'Nadam', 'AdamW'	'Nadam'
Learning rate	0.0001, 0.001, 0.01, 0.1, 0.2	0.01
Momentum	0.0, 0.2, 0.4, 0.6, 0.8, 0.9	0.9

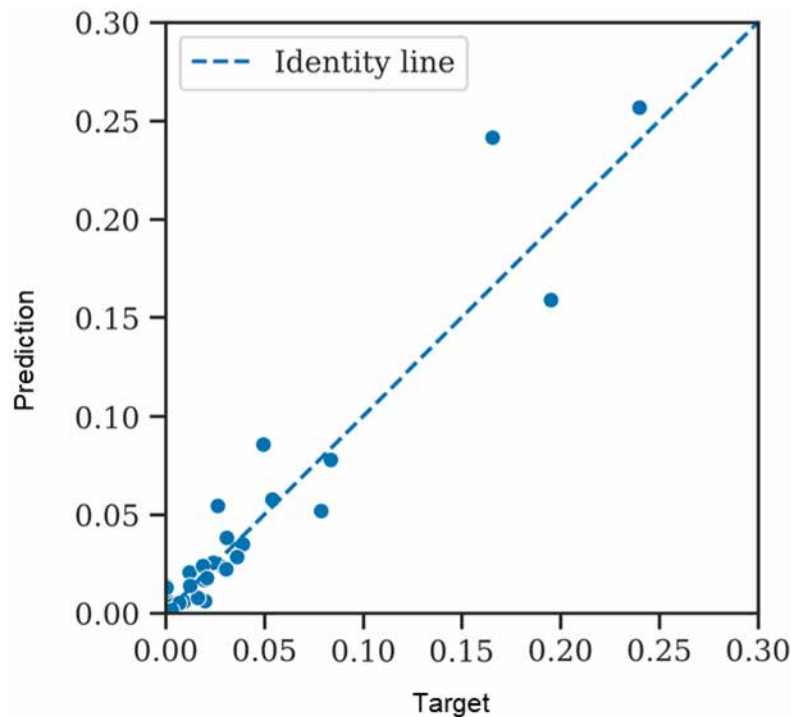


Figure 6—Plots of predictions vs. target values by using the ANN model.

Conclusions

In this study, two popular and powerful machine learning algorithms were comparatively investigated for small data sets with considering fluids properties, proppant properties, and wall retardation effect to predict single proppant settling velocity in HVFRs. Based on the results, the following conclusions can be drawn:

- Expert (or domain) knowledge to conduct preprocessing and quality control of mined data sets in building machine learning models is very important. It is highly recommended to mine training examples from their original literature instead of the papers they are cited.
- An ANN model and an XGBoost model of the settling velocity for single proppant settling in HVFRs are established with the mean absolute errors of 0.010379 and 0.004253 respectively. XGBoost has better performance than ANN with only one hidden layer in terms of selected datasets and has the potential to properly handle missing values by itself.
- The data sets are small in this study due to the availability of some input features, especially for the density of the fluid and relaxation time. More experimental works or data mining from literature are required to increase the size of training examples to fix potential high variance problems. More

features, such as proppant shape and concentration, can be added to training examples to lower bias and increase predicting accuracy.

Nomenclature

d_p	= Particle diameter, m
$F(n)$	= Drag correction factor
$f_2(n)$	= Dimensionless function dependent on the flow behavior index
$f_3(n)$	= Dimensionless function dependent on the flow behavior index
g	= Acceleration due to gravity, m/s ²
K	= Flow consistency index, Pa·S ⁿ
n	= Flow behavior index
p	= Dimensionless coefficient dependent on the particle Weissenberg number
r	= Ration of the particle diameter to the fracture spacing
Re	= Reynolds number
Re_{INEL}	= Reynold number for inelastic power-law fluids
T	= Relaxation time, s
V	= Settling velocity, m/s
V_{EL}	= Settling velocity in unbounded elastic fluids, m/s
$V_{ELConfined}$	= Settling velocity in confined elastic fluids, m/s
V_{INEL}	= Settling velocity in unbounded inelastic fluids, m/s
W	= Fracture width, m
We_{EL}	= Weissenberg number of the particle settling in unbounded elastic fluids
We_{INEL}	= Weissenberg number of the particle settling in unbounded inelastic fluids
ρ_f	= Density of the fluid, kg/m ³
ρ_p	= Density of the particle, kg/m ³
μ	= Apparent viscosity of the fluid, Pa·S

References

- Abdullah, M. B., Delshad, M., Sepehrnoori, K. et al. 2023. Physics-Based and Data-Driven Polymer Rheology Model. *SPE Journal*, 1–23. <https://doi.org/10.2118/214307-PA>.
- Acharya, A. R. 1988. Viscoelasticity of Crosslinked Fracturing Fluids and Proppant Transport. *SPEPE* November: 483–488.
- Amipally, S. K. and Kuru, E. 2018. Settling Velocity of Particles in Viscoelastic Fluids: A Comparison of the Shear-Viscosity and Elasticity Effects. *SPE J.* **23** (5): 1689–1705. SPE-187255-PA. <https://doi.org/10.2118/187255-PA>.
- Biheri, G. and Imqam, A. 2021. Experimental Study: High Viscosity Friction Reducer Fracture Fluid Rheological Advantages Over the Guar Linear Gel. Paper presented at the 55th U.S. Rock Mechanics/Geomechanics Symposium, Virtual, June 2021. ARMA-2021-1814.
- Biheri, G. and Imqam, A. 2021. Settling of Spherical Particles in High Viscosity Friction Reducer Fracture Fluids. *Energies* **14**, no. 9: 2462. <https://doi.org/10.3390/en14092462>.
- Biheri, G. and Imqam, A. 2022. Proppant Transport Using High-Viscosity Friction Reducer Fracture Fluids at High-Temperature Environment. *SPE J.* **27** (01): 60–76. SPE-206750-PA. <https://doi.org/10.2118/206750-PA>.
- Ge, X., Biheri, G., and Imqam, A. 2022. Laboratory Comparative Study of Anionic and Cationic High-Viscosity Friction Reducers in Moderate to Extremely High Total Dissolved Solids Environments. *SPE J.* <https://doi.org/10.2118/212298-PA>.
- Ge, X., Biheri, G., and Imqam, A. 2022. Proppant Transport Analysis of the Anionic High Viscosity Friction Reducer in High-TDS Marcellus Shale Formation Water Environments. Paper presented at the SPE Eastern Regional Meeting, Wheeling, West Virginia, USA, October 2022. <https://doi.org/10.2118/211884-MS>.
- Kelessidis, V.C., 2003. Terminal velocity of solid spheres falling in Newtonian and nonNewtonian liquids. *Tech. Chron. Sci. J. T.C.G.* **24** (1 & 2), 43–54.
- Kelessidis, V.C., Mpandelis, G.E., 2004. Measurements and prediction of terminal velocity of solid spheres falling through stagnant pseudoplastic liquids. *Powder Technol.* **147**, 117–125.

- Lu, R. 2020. *Application of machine learning to gas flaring (Doctoral dissertation, Colorado School of Mines, United States)*. Retrieved from <https://hdl.handle.net/11124/176331>.
- Malhotra, S. 2010. *Proppant settling in viscoelastic surfactant (VES) fluids (Doctoral dissertation)*. Retrieved from <http://hdl.handle.net/2152/ETD-UT-2010-12-2412>.
- Malhotra, S. and Sharma, M. M. 2011. A General Correlation for Proppant Settling in VES Fluids. Paper presented at the SPE Hydraulic Fracturing Technology Conference, The Woodlands, Texas, USA, January 2011. <https://doi.org/10.2118/139581-MS>.
- McCabe, W. L., Smith, J. C., and Harriott, P. 2004. *Unit Operations of Chemical Engineering*, New York City: McGraw-Hill.
- Rao, H., Shi, X., Rodrigue, A.K. et al. 2019. Feature selection based on artificial bee colony and gradient boosting decision tree. *Appl. Soft Comput. J.* **74**, 634–642. <https://doi.org/10.1016/j.asoc.2018.10.036>.
- Stokes, G. G. 1851. *On the Effect of the Internal Friction of Fluids on the Motion of Pendulums*. Cambridge, UK: Pitt Press.
- Yao, S., Chang, C., Hai, K. et al. 2022. A review of experimental studies on the proppant settling in hydraulic fractures. *Journal of Petroleum Science and Engineering*, **208**, 109211. <https://doi.org/10.1016/j.petrol.2021.109211>.
- Yu, L., and Liu, H. 2004. Efficient feature selection via analysis of relevance and redundancy. *The Journal of Machine Learning Research*, **5**, 1205–1224.
- Zhu, Z., Song, X., Yao, X. et al. 2021. Intelligent Prediction of Settling Velocity for Arbitrary Shape Particles in Vertical Fractures. Paper presented at the 55th U.S. Rock Mechanics/Geomechanics Symposium, Virtual, June 2021.

Appendix A

Table A-1 presents modified data sets used for this study with missing values manually imputed by the best approximation based on the information provided within literatures.

Table A-1—Data sets used for this study with missing values manually imputed.

Input features							Output features
K (Pa·S ⁿ)	n	d_p (m)	ρ_s (kg/m ³)	ρ_f (kg/m ³)	Relaxation time, T(s)	Fracture width, W (m)	Velocity, V (m/s)
Kelessidis (2003)							
0.2648	0.7529	0.0015	2260	1000	0	0.1	0.0119
0.2648	0.7529	0.0021	2727	1000	0	0.1	0.0361
0.2648	0.7529	0.0023	2449	1000	0	0.1	0.0409
0.2648	0.7529	0.003	2609	1000	0	0.1	0.0664
0.2648	0.7529	0.0035	2572	1000	0	0.1	0.0802
0.0353	0.8724	0.0015	2260	1000	0	0.1	0.044
0.0165	0.9198	0.0015	2260	1000	0	0.1	0.0597
0.0353	0.8724	0.0021	2727	1000	0	0.1	0.1008
0.0353	0.8724	0.0023	2449	1000	0	0.1	0.1119
0.0165	0.9198	0.0021	2727	1000	0	0.1	0.1275
0.0353	0.8724	0.003	2609	1000	0	0.1	0.1592
0.0165	0.9198	0.0023	2449	1000	0	0.1	0.1403
0.0353	0.8724	0.0035	2572	1000	0	0.1	0.1825
0.0165	0.9198	0.003	2609	1000	0	0.1	0.195
0.0165	0.9198	0.0035	2572	1000	0	0.1	0.2196
Kelessidis and Mpandelis (2004)							
0.001	1	0.0032	2506	1000	0	0.1	0.3692
0.001	1	0.0022	2668	1000	0	0.1	0.2935
0.001	1	0.0012	2314	1000	0	0.1	0.1763
0.001	1	0.0026	11444	1000	0	0.1	1.066
0.135	1	0.0032	2506	1000	0	0.1	0.042
0.135	1	0.0022	2668	1000	0	0.1	0.0232
0.135	1	0.0012	2314	1000	0	0.1	0.0072
0.135	1	0.0026	11444	1000	0	0.1	0.1848

Input features						Output features	
0.135	1	0.0031	7859	1000	0	0.1	0.1656
0.1152	0.7449	0.0032	2506	1000	0	0.1	0.1282
0.1152	0.7449	0.0022	2668	1000	0	0.1	0.0835
0.1152	0.7449	0.0012	2314	1000	0	0.1	0.0321
0.1152	0.7449	0.0026	11444	1000	0	0.1	0.4657
0.0865	0.861	0.0032	2506	1000	0	0.1	0.1031
0.0865	0.861	0.0022	2668	1000	0	0.1	0.0637
0.0865	0.861	0.0012	2314	1000	0	0.1	0.0225
0.0865	0.861	0.0026	11444	1000	0	0.1	0.3855
0.0865	0.861	0.0031	7859	1000	0	0.1	0.3399
0.0849	0.9099	0.0032	2506	1000	0	0.1	0.082
0.0849	0.9099	0.0022	2668	1000	0	0.1	0.0493
0.0849	0.9099	0.0012	2314	1000	0	0.1	0.0164
0.0849	0.9099	0.0026	11444	1000	0	0.1	0.3286
0.0849	0.9099	0.0031	7859	1000	0	0.1	0.2828
Molhotra (2010)							
0.363	0.484	0.00174	2510	1000	0.171	0.11	0.02
0.363	0.484	0.00203	2510	1000	0.171	0.11	0.025
0.363	0.484	0.00294	2510	1000	0.171	0.11	0.045
0.363	0.484	0.00363	2510	1000	0.171	0.11	0.055
0.363	0.484	0.00417	2510	1000	0.171	0.11	0.06
0.363	0.484	0.00174	2510	1000	0.171	0.008	0.018
0.363	0.484	0.00203	2510	1000	0.171	0.008	0.02
0.363	0.484	0.00294	2510	1000	0.171	0.008	0.036
0.363	0.484	0.00363	2510	1000	0.171	0.008	0.0451
0.363	0.484	0.00417	2510	1000	0.171	0.008	0.054
0.363	0.484	0.00174	2510	1000	0.171	0.0036	0.015
0.363	0.484	0.00203	2510	1000	0.171	0.0036	0.01775
0.363	0.484	0.00294	2510	1000	0.171	0.0036	0.02925
0.472	0.389	0.00174	2510	1000	0.389	0.11	0.015
0.472	0.389	0.00203	2510	1000	0.389	0.11	0.019
0.472	0.389	0.00294	2510	1000	0.389	0.11	0.036

Input features					Output features		
0.472	0.389	0.00363	2510	1000	0.389	0.11	0.045
0.472	0.389	0.00417	2510	1000	0.389	0.11	0.051
0.472	0.389	0.00174	2510	1000	0.389	0.008	0.0135
0.472	0.389	0.00203	2510	1000	0.389	0.008	0.01615
0.472	0.389	0.00294	2510	1000	0.389	0.008	0.0288
0.472	0.389	0.00363	2510	1000	0.389	0.008	0.03645
0.472	0.389	0.00417	2510	1000	0.389	0.008	0.0408
0.472	0.389	0.00174	2510	1000	0.389	0.0036	0.01125
0.472	0.389	0.00203	2510	1000	0.389	0.0036	0.01425
0.472	0.389	0.00294	2510	1000	0.389	0.0036	0.0234
0.336	0.579	0.00171	2510	1000	0.555	0.11	0.0075
0.336	0.579	0.00198	2510	1000	0.555	0.11	0.0085
0.336	0.579	0.00297	2510	1000	0.555	0.11	0.0175
0.336	0.579	0.00363	2510	1000	0.555	0.11	0.0225
0.336	0.579	0.00417	2510	1000	0.555	0.11	0.0265
0.336	0.579	0.00171	2510	1000	0.555	0.008	0.006825
0.336	0.579	0.00198	2510	1000	0.555	0.008	0.008415
0.336	0.579	0.00297	2510	1000	0.555	0.008	0.015925
0.336	0.579	0.00363	2510	1000	0.555	0.008	0.019125
0.336	0.579	0.00417	2510	1000	0.555	0.008	0.021465
0.336	0.579	0.00171	2510	1000	0.555	0.0036	0.005925
0.336	0.579	0.00198	2510	1000	0.555	0.0036	0.006885
0.336	0.579	0.00297	2510	1000	0.555	0.0036	0.01225
0.785	0.771	0.00171	2510	1000	0.31	0.11	0.005
0.785	0.771	0.00198	2510	1000	0.31	0.11	0.0065
0.785	0.771	0.00297	2510	1000	0.31	0.11	0.0145
0.785	0.771	0.00363	2510	1000	0.31	0.11	0.021
0.785	0.771	0.00417	2510	1000	0.31	0.11	0.0275
0.785	0.771	0.00198	2510	1000	0.31	0.008	0.005265
0.785	0.771	0.00297	2510	1000	0.31	0.008	0.012325
0.785	0.771	0.00363	2510	1000	0.31	0.008	0.0168
0.785	0.771	0.00417	2510	1000	0.31	0.008	0.022

Input features							Output features
0.785	0.771	0.00171	2510	1000	0.31	0.0036	0.00335
0.785	0.771	0.00198	2510	1000	0.31	0.0036	0.004485
0.785	0.771	0.00297	2510	1000	0.31	0.0036	0.006815
0.876	0.7395	0.00174	2510	1000	0.284	0.11	0.0045
0.876	0.7395	0.00203	2510	1000	0.284	0.11	0.0055
0.876	0.7395	0.00294	2510	1000	0.284	0.11	0.0125
0.876	0.7395	0.00363	2510	1000	0.284	0.11	0.018
0.876	0.7395	0.00417	2510	1000	0.284	0.11	0.024
0.876	0.7395	0.00174	2510	1000	0.284	0.008	0.00396
0.876	0.7395	0.00203	2510	1000	0.284	0.008	0.004455
0.876	0.7395	0.00294	2510	1000	0.284	0.008	0.01075
0.876	0.7395	0.00363	2510	1000	0.284	0.008	0.01458
0.876	0.7395	0.00417	2510	1000	0.284	0.008	0.01968
0.876	0.7395	0.00174	2510	1000	0.284	0.0036	0.00288
0.876	0.7395	0.00203	2510	1000	0.284	0.0036	0.003355
0.876	0.7395	0.00294	2510	1000	0.284	0.0036	0.005875
2.83	0.9805	0.00171	2510	1000	0.212	0.11	0.001
2.83	0.9805	0.00198	2510	1000	0.212	0.11	0.0013
2.83	0.9805	0.00297	2510	1000	0.212	0.11	0.0027
2.83	0.9805	0.00363	2510	1000	0.212	0.11	0.0036
2.83	0.9805	0.00417	2510	1000	0.212	0.11	0.0046
2.83	0.9805	0.00171	2510	1000	0.212	0.008	0.0009
2.83	0.9805	0.00198	2510	1000	0.212	0.008	0.001235
2.83	0.9805	0.00297	2510	1000	0.212	0.008	0.002295
2.83	0.9805	0.00363	2510	1000	0.212	0.008	0.002736
2.83	0.9805	0.00417	2510	1000	0.212	0.008	0.003726
2.83	0.9805	0.00171	2510	1000	0.212	0.0036	0.00074
2.83	0.9805	0.00198	2510	1000	0.212	0.0036	0.000819
2.83	0.9805	0.00297	2510	1000	0.212	0.0036	0.00207
2.792	0.9755	0.00174	2510	1000	0.227	0.11	0.0012
2.792	0.9755	0.00203	2510	1000	0.227	0.11	0.0015
2.792	0.9755	0.00294	2510	1000	0.227	0.11	0.0031

Input features						Output features	
2.792	0.9755	0.00363	2510	1000	0.227	0.11	0.0041
2.792	0.9755	0.00417	2510	1000	0.227	0.11	0.0053
2.792	0.9755	0.00174	2510	1000	0.227	0.008	0.00108
2.792	0.9755	0.00203	2510	1000	0.227	0.008	0.00138
2.792	0.9755	0.00294	2510	1000	0.227	0.008	0.002573
2.792	0.9755	0.00363	2510	1000	0.227	0.008	0.00287
2.792	0.9755	0.00417	2510	1000	0.227	0.008	0.003445
2.792	0.9755	0.00174	2510	1000	0.227	0.0036	0.00072
2.792	0.9755	0.00203	2510	1000	0.227	0.0036	0.00087
2.792	0.9755	0.00294	2510	1000	0.227	0.0036	0.001395
23.75	0.9645	0.00174	2510	1000	2.245	0.11	0.00009
23.75	0.9645	0.00203	2510	1000	2.245	0.11	0.00012
23.75	0.9645	0.00294	2510	1000	2.245	0.11	0.00022
23.75	0.9645	0.00363	2510	1000	2.245	0.11	0.00028
23.75	0.9645	0.00417	2510	1000	2.245	0.11	0.00035
Arnipally and Kuru (2018)							
0.27	0.35	0.002	2510	998	12	0.11	0.0307
0.27	0.35	0.0025	8050	998	12	0.11	0.18
0.27	0.35	0.00118	2510	998	12	0.11	0.0052
0.27	0.35	0.0015	2510	998	12	0.11	0.0163
0.27	0.35	0.003	2510	998	12	0.11	0.0788
0.25	0.36	0.002	2510	997	50	0.11	0.0144
0.25	0.36	0.0025	8050	997	50	0.11	0.06
0.25	0.36	0.00118	2510	997	50	0.11	0.0034
0.25	0.36	0.0015	2510	997	50	0.11	0.0093
0.25	0.36	0.003	2510	997	50	0.11	0.0353
0.26	0.35	0.002	2510	997	110	0.11	0.0084
0.26	0.35	0.0025	8050	997	110	0.11	0.04
0.26	0.35	0.00118	2510	997	110	0.11	0.0025
0.26	0.35	0.0015	2510	997	110	0.11	0.0058
0.26	0.35	0.003	2510	997	110	0.11	0.022
0.16	0.38	0.002	2510	998	12	0.11	0.039

Input features						Output features	
0.16	0.38	0.00118	2510	998	12	0.11	0.0114
0.16	0.38	0.0015	2510	998	12	0.11	0.0245
0.16	0.38	0.003	2510	998	12	0.11	0.0916
0.27	0.35	0.002	2510	998	12	0.11	0.0307
0.27	0.35	0.00118	2510	998	12	0.11	0.0052
0.27	0.35	0.0015	2510	998	12	0.11	0.0163
0.27	0.35	0.003	2510	998	12	0.11	0.0788
0.35	0.38	0.002	2510	1005	12	0.11	0.011
0.35	0.38	0.00118	2510	1005	12	0.11	0.0017
0.35	0.38	0.0015	2510	1005	12	0.11	0.0049
0.35	0.38	0.003	2510	1005	12	0.11	0.0294
Biheri and Imqam 2022							
0.79	0.31	0.006	2626	1000	21.32	0.01	0.042
0.79	0.31	0.006	2626	1000	21.32	0.007	0.031
0.79	0.31	0.004	2626	1000	21.32	0.01	0.026
0.79	0.31	0.002	2626	1000	21.32	0.01	0.0012
0.71	0.28	0.006	2626	1000	5.95	0.01	0.16
0.41	0.31	0.006	2626	1000	0.2	0.01	0.19
0.09	0.74	0.006	2626	1000	0.044	0.01	0.21
0.09	0.74	0.006	2626	1000	0.044	0.007	0.16
0.09	0.74	0.004	2626	1000	0.044	0.01	0.16
0.09	0.74	0.002	2626	1000	0.044	0.01	0.05
0.05	0.78	0.006	2626	1000	0.02	0.01	0.24
0.02	0.86	0.006	2626	1000	0	0.01	0.28
Ge and Imqam 2022							
0.84875	0.302	0.000455	3270	1200	12.077	0.03	0
0.84875	0.302	0.000455	3270	1200	12.077	0.0035	0
0.24193	0.409	0.000455	3270	1200	2.695	0.03	0.0008
0.24193	0.409	0.000455	3270	1200	2.695	0.0035	0.0006
0.032252	0.671	0.000455	3270	1200	0.08	0.03	0.012
0.016433	0.764	0.000455	3270	1200	0.272	0.03	0.021
0.017547	0.763	0.000455	3270	1200	0	0.03	0.019

Input features						Output features	
0.017547	0.763	0.000455	3270	1200	0	0.0035	0.012
0.015389	0.742	0.000455	3270	1200	0	0.03	0.029
0.015389	0.742	0.000455	3270	1200	0	0.0035	0.024
0.016722	0.793	0.000455	3270	1200	0	0.03	0.024
0.022713	0.754	0.000455	3270	1200	0	0.03	0.019
